

PIOTR CZARNOCKI *

DIMENSIONING THE ACCEPTABLE PLY DROP IN FLANGES OF COMPOSITE SPARS USING THE LINEAR FRACTURE MECHANICS APPARATUS

The quest for airframe weight reduction results in a careful dimensioning cross section areas of structural airframe components depending on the anticipated loading. In the case of flanges of polymeric laminate spars subjected to tension such a dimensioning can be done by means of appropriate ply dropping along the spar flanges. A method for an effective calculation of the number of plies that can be cut off at the cross-section under consideration without excessive stress concentration resulted has been presented. The method takes advantage of the Linear Fracture Mechanics tools combined with simple finite element calculations. In addition, experimental data needed can be easily obtained with the use of inexpensive specimens that are simple for manufacturing and testing.

1. Introduction

The quest for airframe weight reduction usually results in a careful dimensioning cross section areas of structural airframe components depending on the anticipated loading. In the case of polymeric laminate spars, such an adjustment can be done by means of appropriate ply dropping along the spar flanges. In a view of strength, the best solution is the ramp-like change in the flange cross-section area, however, it is not practical for manufacturing reasons. For this reason, a step changes are more reasonable. Reduction in a step number simplifies manufacturing process, however, if a number of truncated flange plies is too large at the same flange station, not acceptable stress concentration can be produced. It is very important designer's task to decide what number of plies can be cut off. A suitable method to determine this number is presented hereinafter.

* *Institut of Aeronautics and Applied Mechanics, Warsaw University of Technology, ul. Nowowiejska 24, 00-665 Warsaw, Poland; E-mail: pecz@meil.pw.edu.pl*

It follows from experience that in the case of stepped flanges a failure under tensile loading starts with the delamination caused by an excessive interfacial stress. The delamination originates at a spar discontinuity, Fig.1, and propagates along the flange for several millimetres in the same plane. The failure load can be approximated via interfacial shear stress. Part of the flange with truncated ply can be considered as a long adhesive lap joint, as shown in Fig.1. Therefore, for calculation of the interlaminar shear stress producing delamination, a typical analysis of adhesive joints [1] could be adopted, and an interfacial shear stress could be calculated using formula (1).

$$\tau = \frac{P \cdot G}{t \cdot \lambda \cdot h_1 E_1} \cdot \frac{\cosh \lambda(l - x) - \cosh \lambda x}{\sinh \lambda l} \quad (1)$$

where $\lambda = \sqrt{\frac{G}{t} \left(\frac{1}{h_1 E_1} + \frac{1}{h_2 E_2} \right)}$ and t , h_1 , and h_2 are the thickness of adhesive layer and thicknesses of adherents, respectively

One can show that for a sufficiently long glue line eq. (1) can be approximated with (2) and the failure load P_{cr} corresponding to the ultimate shear stress τ_{max} can be easily calculated.

$$\tau_{max} = \frac{P_{cr} G}{t \lambda h_1 E} \quad (2)$$

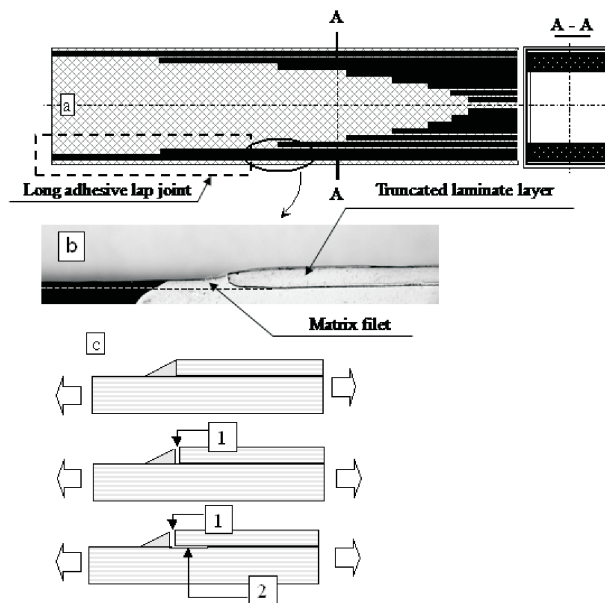


Fig. 1. Wing spar with stepped flanges: general view (a), matrix fillet at the end of truncated ply (b), stages of the fracture process (c)

The formula is simple, however, it is difficult to estimate the glue layer thickness, t . It is not well defined and varies in both the longitudinal and lateral directions. Estimation of t on the basis of the resin volume fraction results in non realistic shear stress [2]. Alternative to the above could be the FEM. In this case, the laminate could be treated as a homogenous orthotropic material, but, to obtain useful results, one must know an exact fillet radius, r_f , at the corner resulting from ply truncation. Unfortunately, fillet radii are matter of chance and can not be defined *a priori*. On the assumption that they are equal to 0, singularity appears at the corner, resulting in infinite stress. Such results are useless from the practical point of view. More effective approach can be offered by the fracture mechanics tools, and that is presented in this paper.

2. Fracture Mechanics Approach

2.1. Mechanism of failure

Schematic representation of a typical composite spar is shown in Fig.1a. Figure 1b presents end region of the truncated ply with a matrix fillet and adhering ply bypassing the cut. For visualisation purposes, the notch region was painted with white brittle lacquer. The dashed line indicates a border line separating the fillet created by flowing out resin and bypassing underneath ply. It follows from experience that a failure starts with the delamination of a truncated ply. The sequence of fracture events is depicted in Fig.1c. At first the slit, denoted by digit 1, separating the fillet and end of top layer is formed. It does not penetrate into the underneath ply. As the load increases, delamination begins and the longitudinal slit, denoted with digit 2, develops in the longitudinal flange direction and splits the adjacent composite layers. Due to such a split, an effective flange cross section decreases, which results in a tensile failure of flange. To prevent that, it is crucial to estimate a critical load corresponding to the delamination onset. Experimental works done on laminates with epoxy matrixes have proved that for such materials the delamination can be predicted with the help of the Linear Fracture Mechanics (LFM). Resistance against delamination can be defined in terms of the critical value of the Strain Energy Release Rate, (SERR), G_c . For composite materials, G_c , is a function of the Phase Angle, Ψ [3,4,5] (3).

$$\Psi = a \tan \sqrt{\frac{G_{II}}{G_I}} \quad (3)$$

Therefore, the application of Fracture Mechanics to the problem under consideration involves the following steps:

- a) analytical or numerical determination of the total value of SERR, G_{tot} , for the assumed interlaminar crack,
- b) determination of the relationship Ψ versus (h_u/h_l) where h_u and h_l are thicknesses of the upper and lower composite layers, respectively
- c) experimental determination of G_c versus Ψ for the composite under consideration,
- d) comparison of the calculated total G_{tot} , and critical, G_c , SERR values

2.2. FE modelling

To solve the problem in question, not only the total value of SERR, G_{tot} , should be known, but also its components G_I and G_{II} to allow for the phase angle calculation with the use of (3). For this reason, the most suitable tool is the Modified Crack Closure Integral Method (MCCIM), [6]. It allows for straightforward determination of G_I and G_{II} components with eqs. (4) and (5) and calculation of G_{tot} according to (6)

$$G_I = \frac{1}{2\Delta S} P_n \delta_n = \frac{1}{2} P_n (u_{B^I} - u_{B^{II}}) \quad (4)$$

$$G_{II} = \frac{1}{2\Delta S} P_v \delta_v = \frac{1}{2} P_v (v_{B^I} - v_{B^{II}}) \quad (5)$$

where, (see Fig.2):

ΔS – increase in the crack area to be closed

u_{B^I}, v_{B^I} – displacements of node B^I in x and y directions, respectively

$u_{B^{II}}, v_{B^{II}}$ – displacements of node B^{II} in x and y directions, respectively

P_n, P_v – nodal forces at node A acting in x and y directions, respectively

$$G_{tot} = G_1 + G_2 \quad (6)$$

To present the method, a parametric 2D finite element model of laminate with crack was constructed with the use of 4 nodes shell orthotropic elements, Fig. 3. Nodal forces at the crack tip were simulated by 1D spring elements. One spring element with the appropriate degree of freedom was used to simulate each nodal force component i.e. for one pair of the corresponding nodes two spring elements were used. The following boundary conditions were set, (Fig. 3a):

for $x=120\text{mm}$ $u = 0$ and

for $y=-4\text{mm}$ $v=0$

for $x=120\text{mm}$ the uniform displacement $u=u_0$ was applied to simulate loading.

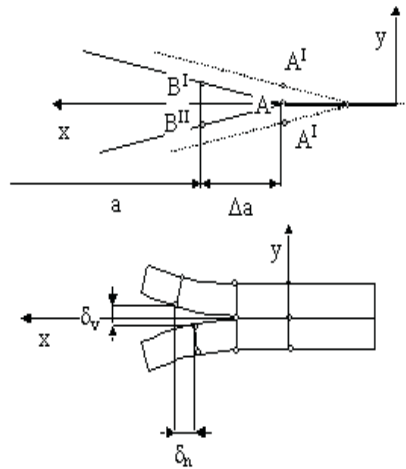


Fig. 2. Crack closure. Definition of the symbols used

The value of u_0 was adjusted in such a way that for each value of $\frac{h_1}{h_2}$ ratio the induced G_{tot} was in the range of expected G_c . The design of mesh in the crack tip region is shown in Fig. 3b. The variable parameter was thickness h_2 (Fig. 3.a) while h_1 was kept constant. The SERR was calculated for $\frac{h_1}{h_2} = 1, 1.33, 2, 4, 8$ and for two values of the Young modulus $E_{11}=E_x=52000, 138000$ MPa.

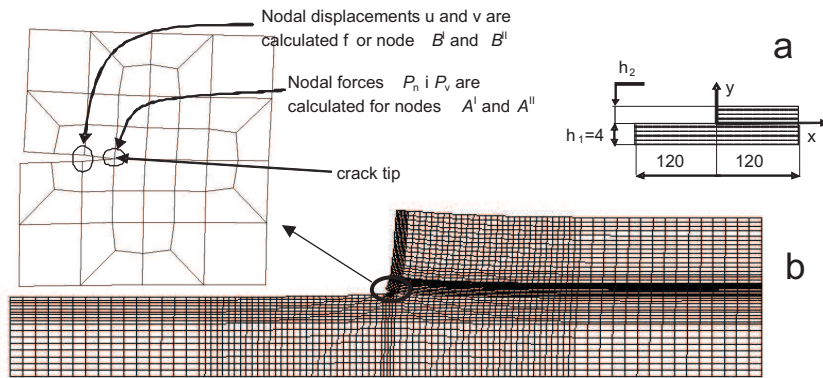


Fig. 3. Finite element model for G_I and G_{II} calculation with the use of MCCI method

To assess the accuracy of numerical results, G_{tot} was calculated for the same range of $\frac{h_1}{h_2}$ ratio with the use of closed form expression (7).

2.3. Closed form expression

For the crack configuration of interest, it is easy to determine G via J integral. As far as LFM is applicable, the J integral and SERR values equal to each other. For efficient calculation of J , one can consider path ABCDEF, Fig. 4. External loading acting in the front of AB cross-section of the laminate layer of thickness h_1 can be expressed in terms of strain, ε_1 , and the total value of SERR can be calculated according to (7).

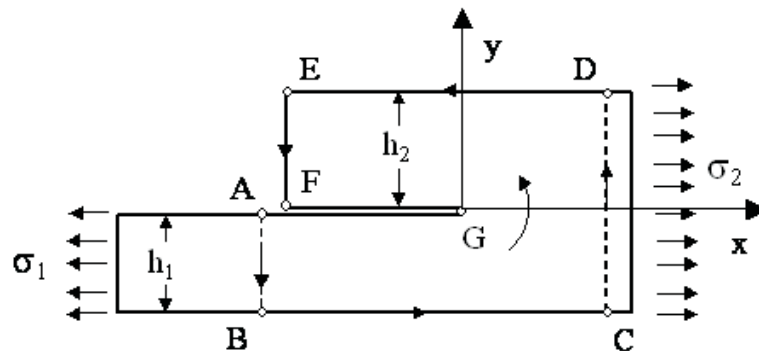


Fig. 4. Suitable path for the calculation of J integral

$$J = Eh_1\varepsilon_1^2 \left(\frac{h_2}{h_1 + h_2} \right) = G_{tot} \quad (7)$$

where E is the Young modulus of laminate in spar longitudinal direction

Unfortunately, that approach does not allow for the determination of $G=f(\Psi)$ relationship.

3. Calculation results

The results obtained are presented in Figs. 5 and 6. The diagram in Fig.5 presents variation of the total value of SERR, G_{tot} , with the geometry of notch created by truncation of plies. The total value of SERR, G_{tot} , is normalised with respect to $Eh_1\varepsilon_1^2$ to allow for the determination of G_{tot} for any value of h_1 and $E_x \equiv E$. the results obtained from the FE model and those calculated using close form solution (7) are in good agreement. The diagrams in Fig. 6 were obtained with the same FE models and represent the variations in the phase angle with the notch geometry for E_x equals to 52000 and 138000 MPa. It is clear that the effect of Young modulus is weak and the increase in its value by the factor of two changes the phase angle, Ψ , by about 3.5° only. Additionally, the effect of $\frac{h_1}{h_2}$ ratio on the phase angle weakens with decreasing thickness of the truncated plies, h_2 .

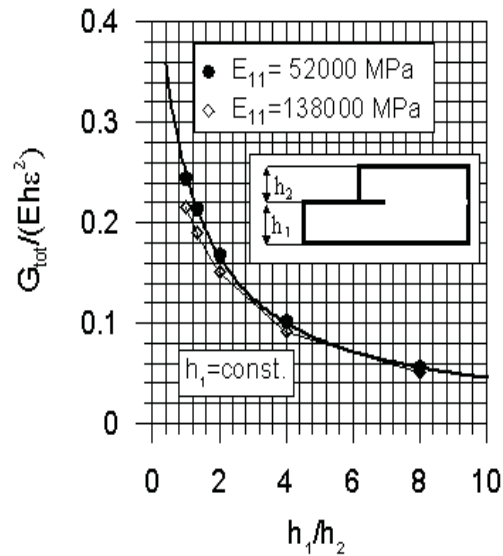


Fig. 5. Variation of SERR with the thickness of truncated laminate layer, h_2 . Continuous line represents the results of closed form solution (eq.7). Numerical results are marked with \circ ($E_x=52000$ MPa) and \diamond ($E_x=138000$ MPa)

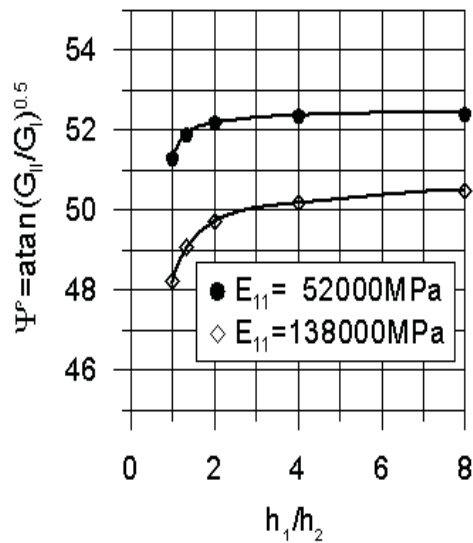


Fig. 6. Variation in the phase angle with the thickness of truncated laminate plies of thickness, h_2

4. Fracture criterion – experimental determination of G_c (Ψ)

4.1. Specimen configuration

Several methods can be used to determine $G_c = f(\Psi)$ for a mixed mode loading [7,8,9]. One of them is the method based on the Single Leg Bending

(SLB) specimen loading configuration [7]. That configuration can cover the phase angle range under consideration and does not require any jig of particular design. The SLB configuration is shown in Fig. 7. The Phase Angle, Ψ , is calculated according to (8)

$$\Psi = a \tan \sqrt{\frac{G_{II}}{G_I}} = a \tan \sqrt{\frac{3}{\left(\frac{H}{h}\right)^2 \left(\frac{H}{h} - 1\right)^2}} \quad (8)$$

where:

H – total thickness of the specimen

h – thickness of the loaded leg

This relationship is presented in Fig. 7 for $\Psi=30^\circ, 45^\circ, 56^\circ$ and 61°

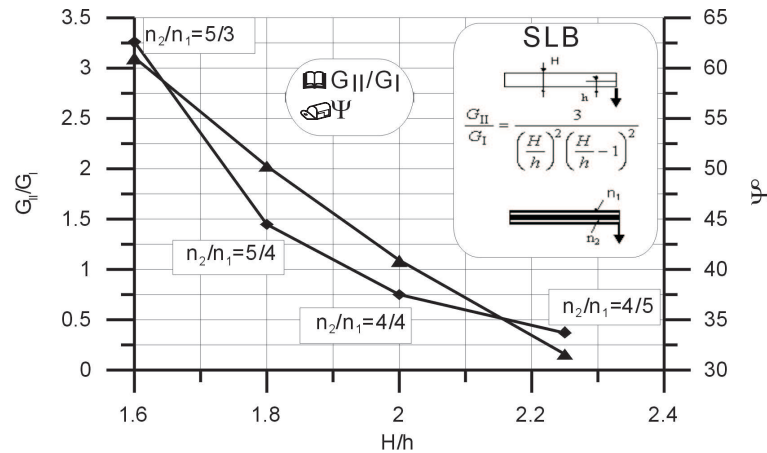


Fig. 7. Relationship $\Psi(H/h)$ for the SLB specimen configuration. The load free leg is composed of n_1 and the loaded leg of n_2 plies, respectively

4.2. Specimens

The geometry of specimens is shown in Fig. 8. The specimens were made of CFRP with the use of Sigratex KDU1034 carbon fibre tape impregnated with L285 epoxy resin. To form the laminate, a wet lay-up technique was used. A profile of the applied cure cycle is shown in Fig. 9. Table 1 presents number of layers used for load free and loaded legs n_1 and n_2 , respectively.

For each H/h ratio, eight specimens were cut out from the same batch according to the trace shown in Fig. 8, to assure reproducibility of material mechanical properties.

Table 1.

n_1	n_2	H/h
5	4	2.25
4	4	2
4	5	1.8
3	5	1.6

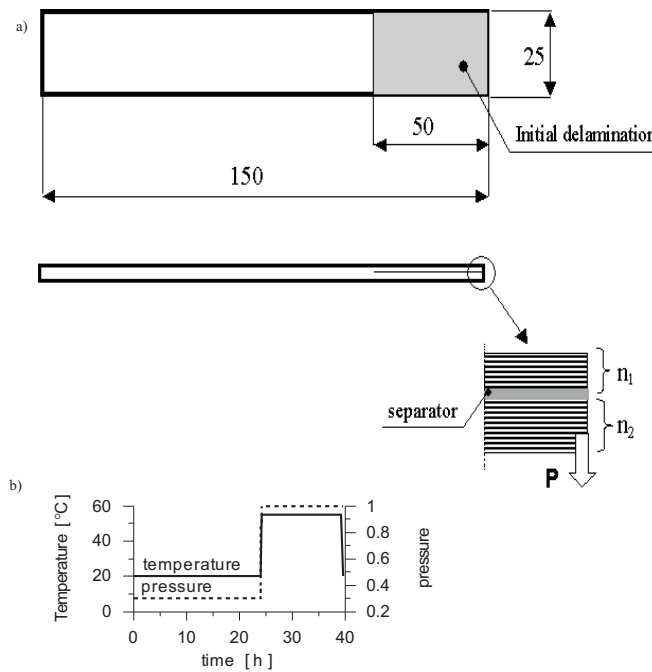


Fig. 8. Geometry of SLB specimens (a) and the profile of curing cycle for Sigratex KDU1034 carbon fibre tape impregnated with L285 epoxy resin (b)

4.3. Tests and results

The tests were run at room temperature with the use of INSTRON machine under controlled displacement conditions with the cross head speed equal to 5mm/min. The examples of typical Load-Displacement diagrams are shown in Fig. 9. The SERR components G_I and G_{II} were calculated with the use of equations

$$G_I = \frac{\omega P^2 a^2}{4BEI} \frac{R}{R + 1} \quad (9)$$

$$G_{II} = \frac{\omega P^2 a^2}{4BEI} \frac{1}{R+1} \tag{10}$$

where

$$I = \frac{B(h_1^3 + h_2^3)}{24} \quad R = \frac{1}{3} \left(\frac{h_1}{h_2}\right)^2 \left(1 + \frac{h_1}{h_2}\right)^2 \quad \omega = \left(\frac{h_1}{h_3}\right)^3 + \frac{3h_1h_2}{(h_1 + h_2)^2}$$

In majority of the tests, the critical value of P corresponding to the crack propagation onset was well defined with the sudden load drop. The P_{cr} values were taken as equal to the maximum load values taken from the load vs. displacement diagrams. In the case of non-linear load-displacement relationships, the C+5% compliance line was drawn and if P_{max} corresponded to a compliance value higher than C+5% the test was assumed to be not-valid.

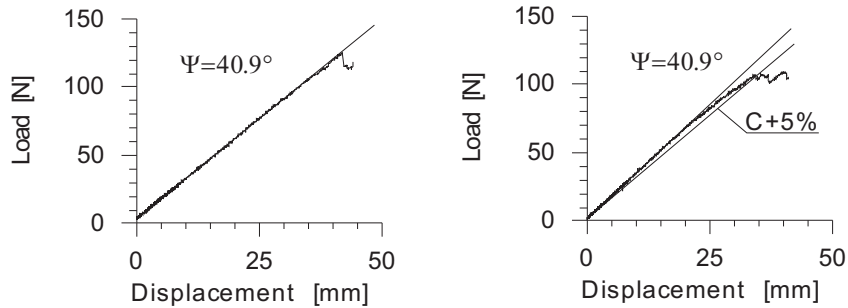


Fig. 9. Typical load-displacement diagrams for SLB tests

The test results are presented in Fig. 10. For each value of Ψ the mean value of G_{tot} and 95% confidence level are indicated.

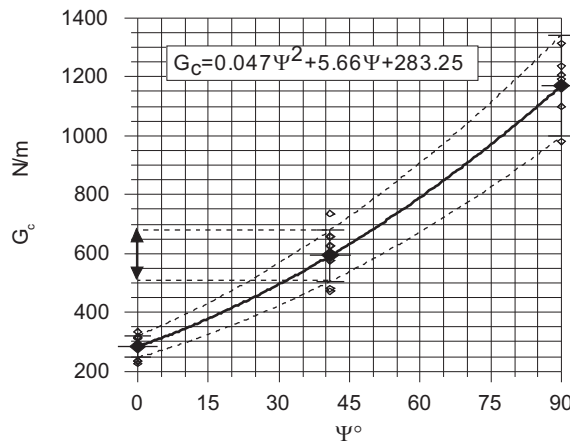


Fig. 10. Results of G_c versus Ψ tests with 95% confidence limit marked

5. Experimental accuracy verification of the method put forward

Application of the presented approach was experimentally verified with the use of coupons representing a segment of flange, Fig. 11. Two coupons were tested. The coupons were made of the same composite system that had been used for SLB specimens. The coupons consisted of core layers of total thickness $2h_1$ and two laps of thickness h_2 each, representing the truncated flange layers. The number of plies used for the core was $2n_1 = 8$ and for each lap $n_2 = 3$

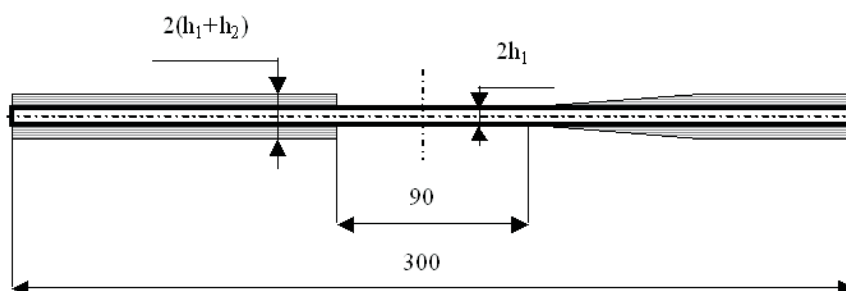


Fig. 11. Specimen representing flange segment in the region of layer truncation. The notch is a result of dropping the external layers of thickness h_2

The tests were run at room temperature. The coupons were loaded in tension under displacement controlled conditions with CHS equal to 1mm/min. For visualisation purposes, of crack initiation the sides of coupons were painted with white brittle lacquer and monitored with a travelling microscope. The obtained stress-displacement diagrams and the critical load values of 31 447 N and 37452 N corresponding to the onset of delamination are shown in Fig. 12.

6. Discussion of results

For the applied coupon geometry, the $\frac{h_1}{h_2}$ ratio equals 1.33. From other tests it is known that for the laminate under consideration the average value of longitudinal Young modulus is 77000 MPa. Using those numbers and the diagram presented in Fig. 5, one can predict the critical load corresponding to the delamination onset. From the diagram in Fig. 5 follows that for $\frac{h_1}{h_2} \approx 1.33$ the corresponding value of $\frac{G}{Eh\varepsilon^2}$ ratio is about 0.2. From the diagram in Fig. 6 it follows that for the same value of $\frac{h_1}{h_2}$ ratio the phase angle

$\Psi \approx 51^\circ$. Upon simple rearrangement of eq.(7) and substituting G_c for G_{tot} one can arrive at (11), which allows for determination of critical load, P_{cr} , corresponding to the delamination onset.

$$P_{cr} = \sqrt{\frac{G_c EA^2}{0.2h_1}} \tag{11}$$

After substituting G_c corresponding to 95% confidence level for G_{tot} in (11), one can find the interval of critical load, P_c , expected to start the delamination. From the diagram in Fig.9 one can estimate that for $\Psi \approx 51^\circ$ the interval of G_c values corresponding to 95% confidence level is $780 \frac{N}{m} \leq G_c \leq 1020 \frac{N}{m}$ and it corresponds to $3230 \div 3660 N$ P_{cr} interval. From inspection of the diagrams in Fig. 12 it follows that the experimental values of critical load are very close to the predicted range and that the average value of critical load is inside the predicated range. Nevertheless, to verify the reliability of the suggested method a larger number of test should be carried out in future.

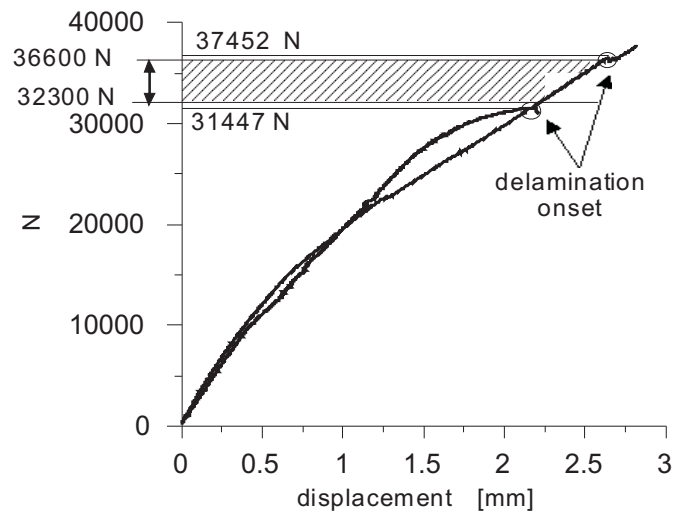


Fig. 12. Results of the tensile tests of the flange segment. Interval of the expected value of P_{cr} is dashed

In author’s opinion, the described method is relatively simple and inexpensive.. It does not involve time consuming FE modelling. When the MCCI method is used, the numerical results are practically insensitive to element size in the crack tip vicinity even for the element dimensions differing by one order of magnitude. It is reported that the length of crack to close, Δa , can be as long as 25% of the total crack length, a , [6].

The experimental data needed can be obtained with the use of simple beam specimens. Such specimens are easy for manufacturing and testing. Also, the data reduction schemes are straightforward.

This work was financially supported by the Ministry of Science and Higher Education in Poland, (Project No. 5 T12C 045 25).

Manuscript received by Editorial Board, February 09, 2009;

REFERENCES

- [1] Van Rijn L.P.V.M.: "Design of Sailplanes Using Composite Materials", in Comprehensive Composite Materials v. 6 pp. 249.
- [2] Czarnocki P.: "Application of fracture mechanics for dimensioning the maximum ply drop in flanges of composite spars", Recent research and design progress in aeronautical engineering and its influence on education, Brno University of Technology, No. 2, 2008.
- [3] Benzeggagh M.L., Kenane M.: "Measurement of Mixed-Mode Delamination Fracture Toughness of Unidirectional Glass/Epoxy Composites with Mixed-Mode Bending Apparatus", Composite Science and Technology, 56, 1996, pp. 439-449.
- [4] Dyson I.N., Kinloch A.J., Okada A.: "The Interlaminar Failure Behaviour of Carbon Fibre/Polyether-ether-ketone Composites", Composites, vol. 25, No. 3, 1994, pp. 189-193.
- [5] Hwu C., Kao C.J., Chang L.E.: "Delamination Fracture Criteria for Composite Laminates". Journal of Composite Materials, vol. 29, No. 15, 1996, pp. 1962-1987.
- [6] Rybicki E.F., Kanninen M.F.: "A finite element calculation of Stress Intensity Factors by a Modified Crack Closure Integral", Engineering Fracture Mechanics, vol. 9, 1977, pp. 931-938.
- [7] Hashemi S., Kinloch A.J., Williams J.G.: "Mechanics and Mechanism of Delamination in Poly(ether-sulphone)/fibre Composite", Composite Science and Technology, 37, 1990, pp. 429-462.
- [8] ASTM D6671-01 Standard test method for Mixed Mode I- Mode II interlaminar Fracture Toughness of Unidirectional Fibre-Reinforced Polymer Matrix Composite.
- [9] Williams J.G.: "The Fracture Mechanics of Delamination Test", Journal of strain Analysis, vol. 24, No. 4, 1989, pp. 207-214.

Wykorzystanie liniowej mechaniki pęknięcia do wyznaczania dopuszczalnych odstopniowań w laminatowych pasach dźwigarów

Streszczenie

Dążenie do redukcji ciężaru płatowca wymaga możliwe dokładnego doboru przekrojów elementów nośnych według spodziewanego obciążenia. W przypadku pasów kompozytowego dźwigara o strukturze laminarnej może to być dokonane na drodze stopniowego gubienia warstw kompozytu. W artykule przedstawiono stosunkowo prostą metodę określania maksymalnej liczby warstw laminatu, która może być odcięta bez powodowania nadmiernej koncentracji naprężeń. W prezentowanej metodzie wykorzystane zostały narzędzia liniowej mechaniki pęknięcia w połączeniu z prostymi obliczeniami prowadzonymi metodą elementów skończonych. Próbkę konieczną do uzyskania wykorzystywanych w tej metodzie stałych materiałowych są łatwe do wykonania a przeprowadzenie samych pomiarów i opracowanie wyników stosunkowo proste.